ACS APPLIED MATERIALS & INTERFACES

Research Article

www.acsami.org

Nanoarchitectures with Controllable Anisotropic Features in Structures and Properties from Simple and Robust Holographic Lithography

Hwan Chul Jeon, Tae Yoon Jeon, and Seung-Man Yang*

National Creative Research Initiative Center for Integrated Optofluidic Systems and Department of Chemical and Biomolecular Engineering, KAIST, Daejeon, 305-701, Korea

Supporting Information

ABSTRACT: Anisotropic nanostructures with precise orientations or sharp corners display unique properties that may be useful in a variety of applications; however, precise control over the anisotropy of geometric features, using a simple and reproducible large-area fabrication technique, remains a challenge. Here, we report the fabrication of highly uniform polymeric and metallic nanostructure arrays prepared using prism holographic lithography (HL) in such a way that the isotropy that can be readily and continuously tuned. The prism position on the sample stage was laterally translated to vary the relative intensities of the four split beams, thereby tuning the isotropy of the resulting polymer nanostructures through the following shapes: circular nanoholes, elliptical nanoholes, and zigzag-shaped nanoarrays. Corresponding large-area, defect-free anisotropic metallic nanostructures could then be fabricated using an HL-featured porous polymer structure as a milling mask. Removal of the polymer mask left zigzag-shaped metallic nanostructure arrays in which nanogaps separated adjacent sharp edges. These structures displayed two distinct optical properties, depending on the direction along which the excitation beam was polarized (longitudinal and transverse modes) incident on the array. Furthermore, bidirectional anisotropic wetting was observed on the anisotropic polymer nanowall array surface.

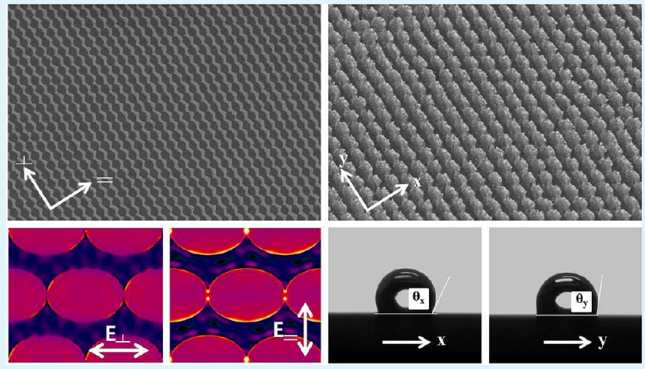

KEYWORDS: *anisotropic nanostructure, holographic lithography, plasmonic, anisotropic wetting*

INTRODUCTION

The fabrication of surfaces with novel anisotropic geometric features is an emerging research area.[1,2] Asymmetrically structured surfaces prepared from a variety of materials can display anisotropic optical properties,[3−5] wetting and adhesion properties,[6−8] thermal responses,[9] electrical conductivities,[10,11] or directional tissue actuation.[12,13] These investigations have inspired fundamental studies and the development of practical applications in electronics, energy conversion, plasmonics, chemical or biomolecular sensing, and bioengineering for medical devices.[1−17] A variety of lithographic approaches to the fabrication of such anisotropic nanostructures have been proposed, including colloidal lithography,[3,14] nanoimprint lithography,[12] block-copolymer lithography,[15] electron beam lithography,[5] and directional photofluidization lithography;[16,17] however, none of these techniques offer robust and simple control over the isotropy of geometric features while also permitting the high-throughput large-area fabrication of structures. Furthermore, conventional photolithography method has difficulties generating periodic sub-micrometer scale structures, because of the diffraction limit and controlling the isotropy of structural features using one type of photomask.

Multi-beam interference lithography, which is a rapid and maskless lithographic technique for fabricating defect-free[18] large-area periodic nanostructure arrays, such as three-dimensional (3D) photonic crystals, is a promising method for generating anisotropic nanostructures.[6,7,19−25] Such nanopatterning strategies rely on the use of optical interference among two or more light beams to transfer a pattern to a prepared photoresist (PR) film.[6,7,18−25] A variety of asymmetric nanostructures have been developed by varying certain controllable optical properties during a lithography process, such as the illumination wave vector,[19−21] phase shift,[22,23] rotational angle during multiple exposures,[24] or the intensity distributions of the laser beams.[24,25] However, adjustments to these parameters require the use of complex optical components, such as waveplates, beam splitters, and rotators, and involve complex alignment steps.[19−25] The complexity of the alignment steps places conventional multi-beam interfer-

Received: July 22, 2013
Accepted: September 10, 2013
Published: September 10, 2013

   dx.doi.org/10.1021/am402886a | ACS Appl. Mater. Interfaces 2013, 5, 9791−9797

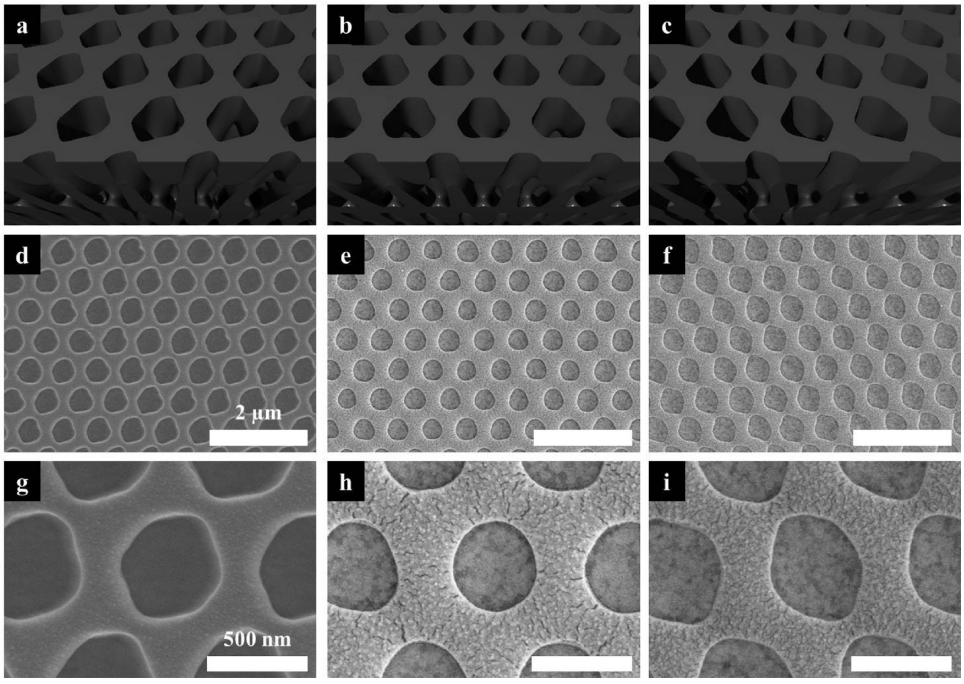

Figure 1. Simulated holographic interference patterns and their predicted effects in the production of periodic nanostructures using a four-beam configuration comprising beams with different intensities that could be tuned based on the prism position: (a) prism position translated right of center, K_1:K_2:K_3 = 0.7:1.3:1; (b) a centered prism position, 1:1:1; and (c) a prism position translated left of center, 1.3:0.7:1. Also shown are large-area and magnified SEM images of three hexagonally ordered polymer nanohole arrays formed from the following prism positions: (d, g) translated right of center, (e, h) centered, and (f, i) translated left of center.

ence lithography techniques at a crucial disadvantage for the commercial fabrication of anisotropic surface features.

In this paper, we report a promising novel and simple strategy for fabricating anisotropic polymeric/metallic nanoarrays with tunable isotropy over a large area via prism holographic lithography (HL) with controllable prism positioning on a sample stage and without the need for additional rearrangement of optical components. The isotropy of a hexagonally ordered polymer nanohole array could be simply tuned by controlling the lateral position of a prism relative to the center of the He−Cd laser beam, thereby varying the relative intensities of the four resulting beams. We furthermore fabricated zigzag-shaped anisotropic metallic nanoarrays over a large area such that nanogaps separated adjacent sharp edges. The nanoarray geometry was determined from the polymer nanostructures used as milling masks. These structures could be prepared by increasing the lateral distance over which the prism position was translated, thereby partially reducing the intensity of the holographic interference patterns. These results agreed well with the simulated data, which predicted the gradual thinning of the partial bridges, resulting finally in disconnection. The anisotropic optical properties of the resulting metallic nanostructures were modeled theoretically using finite-difference time-domain (FDTD) methods. The metallic nanoarrays exhibited two different localized surface plasmon resonance (LSPR) effects, each with different degrees of electric field intensity enhancement, depending on the polarization of the excitation beam (longitudinal and transverse modes).[3−5,26−28] Furthermore, anisotropic polymer nanowall arrays were generated through a combination of prism-controlled HL and etching processes. Bidirectional anisotropic wetting due to the geometric effects was observed based on water contact angle measurements along orthogonal directions on the nanopatterned surfaces.[6,7,25,29]

RESULTS AND DISCUSSION

Anisotropic Polymer Nanostructure Arrays. Our novel method for fabricating anisotropic polymer nanostructure arrays involved single prism HL with controllable prism positioning on a sample stage (see Figure S1a in the Supporting Information). In particular, prism HL is a simple route for fabricating periodic 3D nanostructures using novel prism to create multiple beams from a single laser beam, as compared with conventional multi-beam HL.[29−34] The optical setup for achieving prism HL included a 325-nm He−Cd laser with a 10× beam expander, an electronic beam shutter, and a sample stage, as reported previously by our research group.[29−34] An expanded laser beam (1 cm beam diameter) normally incident on the truncated surface of the top-cut prism passed through the prism and was split into four beams comprising one central beam with a wave vector k_0 and three beams with k_j (j = 1−3), refracted from the side planes (see Figure S1b in the Supporting Information).[30−34] The four beams were recombined on the bottom surface of the prism, and the interference patterns were transferred to a pre-coated SU-8 PR film.

Desired photonic crystals with an asymmetric face-centered cubic (FCC) lattice were prepared using a specially designed prism that yielded a given intensity among the three surrounding beams K_j (j = 1−3) and a higher intensity central beam, K_0, such that the intensity ratios were K_0:K_1:K_2:K_3 = 5.5:1:1:1.[30−34] Here, the relative intensities of the three surrounding beams could be controlled simply by adjusting the prism position on the sample stage while fixing K_0 to a value of 5.5, without the need for additional optical components (see Figure S1a in the Supporting Information), unlike conventional

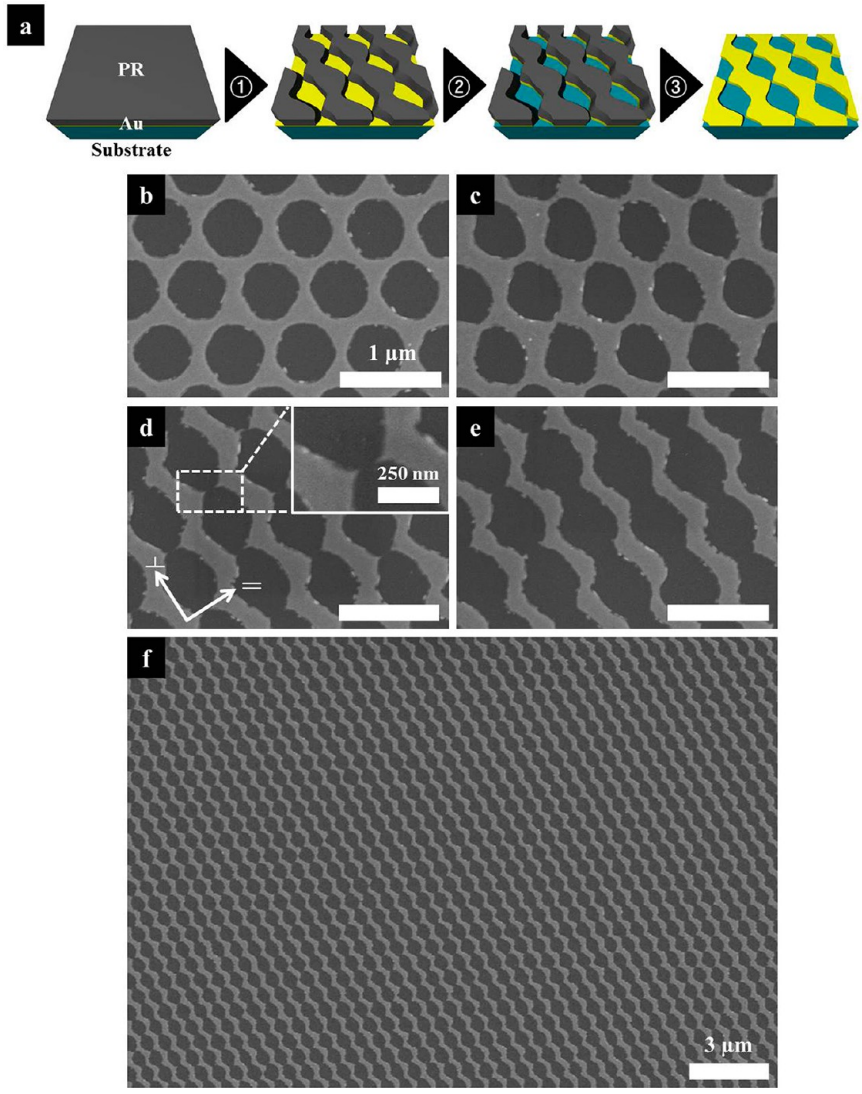

Figure 2. (a) Schematic diagram showing the fabrication of the anisotropic metallic nanostructure arrays using polymer nanostructures produced by prism HL: (1) HL such that the prism position could be controlled and short-time RIE for fabricating the polymer mask on the gold pre-coated substrate; (2) Ar-ion milling to selectively remove the metal thin film from the vacant spaces; (3) long-time RIE to remove the polymer nanostructures. (b–e) SEM images of the metallic nanostructure arrays with an isotropy that could be tuned according to the prism position (the inset in panel (d) depicts a magnified SEM image showing the nanogap distance between sharp corners). (f) Large-area SEM image of the fabricated zigzag-shaped anisotropic metallic nanostructure arrays.

multi-beam interference lithography.[19−25] The intensity variations modulated the partial polymer cross-linking density over an FCC lattice unit formed from the interference pattern.[24,25]

Figures 1a–c show three different simulated 3D interference patterns formed from different prism positions, which resulted in the different intensity ratios between K_1, K_2, and K_3. As shown, the intensity variations of the slanted side beams did not affect the overall lattice form,[24,25] which was a hexagonal packing structure in the (111) plane; however, the variations affected the cross-linking density across the lattice unit, because of the partially different intensity of the interference pattern. A slight shift in the prism position to the right of the center of the coherent beam on the sample stage increased the value of K_2, relative to the value of K_1, yielding a ratio of K_1:K_2:K_3 = 0.7:1.3:1. The overall interference patterns (Figure 1a) then appeared to be slanting to the right, relative to a typical FCC interference pattern obtained from a configuration that yielded a constant intensity ratio among three side beams (K_1:K_2:K_3 = 1:1:1; see Figure 1b). By contrast, an anisotropic periodic pattern with a left-handed slant could be fabricated by shifting the prism position left of center, thereby increasing K_1, relative to K_2 (Figure 1c).

Isotropy-tunable, large-area polymer nanohole arrays were easily obtained via position-controllable prism HL with an appropriate choice of PR thickness.[30−32] Figures 1d–f display scanning electron microscopy (SEM) images of the three types of periodic polymer nanoarrays. The SEM images confirmed that polymer nanohole arrays were well-ordered in a hexagonal pattern with a periodicity of 705 nm over a large area, and the isotropy of the geometric features could be tuned in a straightforward manner. As shown in Figures 1g–i, which display magnified SEM images of the lattice units, the cross-linking density of the interference-based lithographically patterned polymer bridges varied, depending on the prism position, resulting in a variable intensity ratio among the three

side beams (K_1:K_2:K_3). The partial thin polymer bridges were distinguished from the thicker bridges in that they angled the resulting nanostructures to the right (Figure 1g) or the left (Figure 1i), compared to a one-layer FCC structure (Figure 1h). The experimental results of the prism HL method under control over the prism position agreed well with the holographic interference simulation data (see Figures 1a–c).

Furthermore, the distance over which the prism position was laterally translated could be adjusted to generate a continuum of anisotropic nanoarrays (see Figures S1c–e in the Supporting Information). As the prism's lateral translation distance increased, creating a larger difference in the intensity distributions between K_1 and K_2 and changing the ratio from 1.3:0.7 (Figure S1c), to 1.4:0.6 (Figure S1d), to 1.5:0.5 (Figure S1e); as the lateral translation distance increased, the thickness of the interferential partial thin bridges gradually decreased and finally disappeared. The anisotropic nanowall arrays assumed a zigzag shape and could be formed from circular and elliptical nanohole arrays in the (111) plane. We easily obtained a variety of anisotropic nanopatterns in the polymer layer over a large area in such a way that the isotropy could be tuned by making simple adjustments to the prism position on the sample stage during the HL process.

Anisotropic Metallic Nanostructure Arrays. Anisotropic metallic nanoarrays corresponding to the polymer nanohole arrays (Figure 1) could be fabricated using polymer nanostructures as milling masks.[30] The process is illustrated schematically in Figure 2a, which shows the four main steps:

(a) An SU-8 PR layer was spin-coated onto a substrate that had been pre-coated with a thin gold (Au) film. The thickness of the PR layer used to fabricate one-layer FCC structures could be controlled by varying the epoxy-based PR resin concentration and the spin speed.[31]

(b) After soft baking to evaporate the solvent from the polymer film, HL was applied using a specially designed prism with a position that could be controlled relative to the sample stage. After post-exposure baking and development processes, a brief SF_6 reative ion etching (RIE) process was performed to obtain well-defined polymer milling masks by removing the "messy" SU-8 polymer structures.[30]

(c) The thin gold film could be selectively etched from the vacant spaces leaving only the metallic patterns that had been protected by the polymer mask using argon (Ar) ion milling.

(d) A more-extended O_2 RIE process was applied to fully remove the polymer mask from the substrate. Uniform large-area metallic anisotropic arrays with a zigzag shape were thus prepared on the substrate.

Figures 2b–e show SEM images of the various metallic anisotropic nanoarrays that could be formed by varying the distance over which the prism was translated left of center. Metallic nanohole arrays with a periodicity of 705 nm displayed excellent hexagonal order under experimental conditions that were typical for generating one-layer FCC structures; that is, K_1:K_2:K_3 = 1:1:1 (Figure 2b).[30−34] As the prism position was shifted gradually to the left of the laser beam center, the thickness of the resulting metallic bridges, derived from the thin partial polymer bridges used as the milling masks, decreased (Figure 2c) and finally disappeared, leaving isolated nanostructure motifs separated by nanogaps between adjacent sharp corners (Figure 2d). The trend in the nanoarrays structure agreed well with the simulated holographic interference results (see Figures S1c–e in the Supporting Information). The presence of metallic nanogaps in the zigzag-shaped nanostructures can potentially function as "hot spots" for surface-enhanced Raman scattering (SERS) applications, because the magnitude of an electromagnetic (EM) field due to plasmon resonance can be strongly enhanced in the presence of an intergap region, as shown in the inset of Figure 2d (see Figure S2 in the Supporting Information).[5,26−28,30,31] Further translations of the prism position to the left after the nanogaps had formed increased the intergap distance and produced thinner metallic nanostructures (Figure 2e), because the decreased value of K_2 produced lower-intensity regions of partial interference. Figure 2f presents an image confirming that the zigzag-shaped metallic anisotropic nanoarrays covered a large area without defects (an equilateral triangle area with a side length of 0.4 cm), thereby illustrating the main advantage of using prism HL for periodic array fabrication (see Figure S3 in the Supporting Information).[29−34]

The bridge thickness and nanogap distance in the metallic anisotropic nanoarrays were measured from the SEM images using an image analysis program. The results are represented in Figure 3. The graph plotted the bridge thickness (black squares) or nanogap distance (red dots) versus anisotropic metallic arrays as a function of the prism position, shown in Figures 2b–e. Under conditions typically used to fabricate FCC photonic crystals (K_1:K_2:K_3 = 1:1:1),[30−34] all metallic bridges assumed similar thickness values of 118 nm. As the prism position was shifted to the left, the bridge thickness decreased to 54 nm. Finally, the connecting regions of the metallic bridges disappeared and nanogaps with sharp edges formed, separated by distances of 73–246 nm. Overall, the standard variations gradually increased as the prism's lateral translation distance increased. This method is potentially useful for fabricating anisotropic metallic nanoarrays featuring small gaps over a large area through precise control over the prism position on a sample stage.

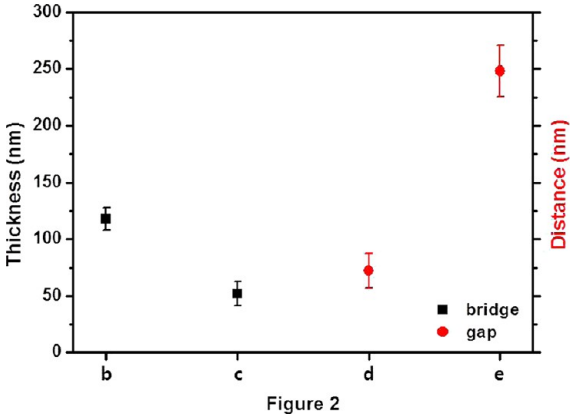

Figure 3. Thickness of the thin bridges and the nanogap distance measured in the metallic nanostructures, as a function of the degree to which the prism position had been shifted off-center.

A configuration in which the prism position was shifted systematically in the opposite (right) direction showed a similar trend. As the prism's lateral translation distance increased, yielding $K_2 > K_1$, the metallic bridges became thinner and finally disappeared (see Figure S4 in the Supporting Information). However, the thinner bridge positions in the

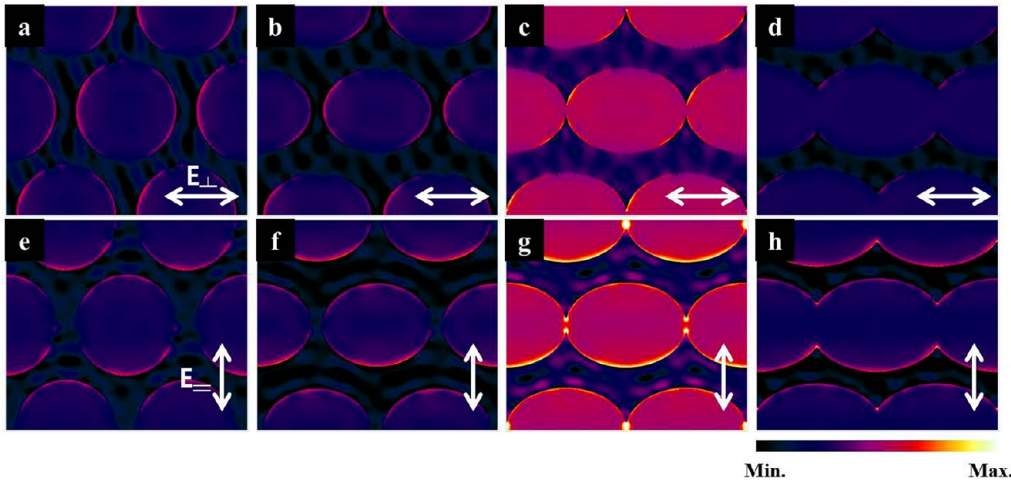

Figure 4. Calculated electric field intensity distributions on the various metallic nanostructure arrays as a function of the prism position, for (a–d) longitudinally polarized or (e–h) transversely polarized excitation beams, plotted using a common intensity colormap. Double-headed arrows indicate the direction along with the incident light was polarized.

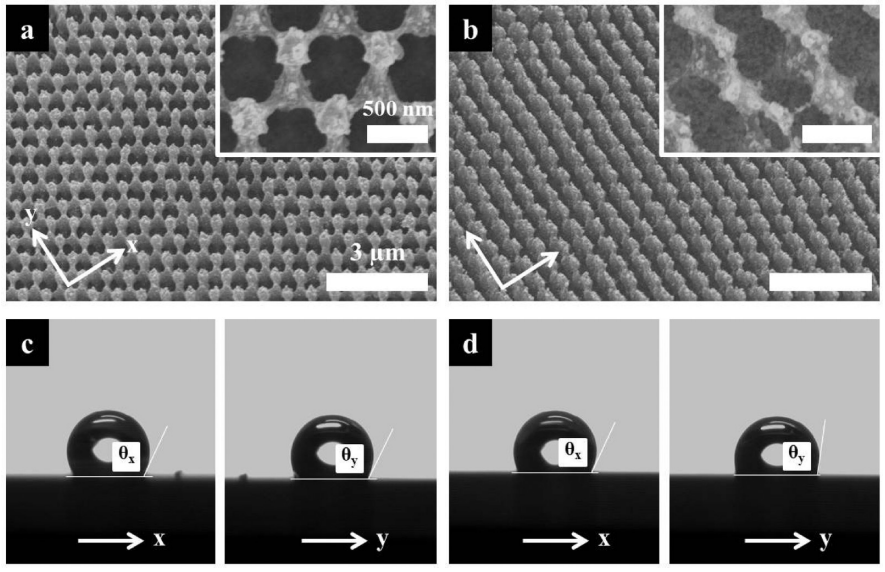

Figure 5. 30° tilted large-area SEM images of (a) the fabricated polymer nanotip and (b) the anisotropic polymer nanowall arrays prepared using HL, such that the prism position could be controlled. The insets show magnified SEM images in the (111) plane. Water contact profiles showing the (c) isotropic or (d) anisotropic wetting properties on the surfaces shown in panel (a) or panel (b), respectively.

lattice unit produced by the right-sided prism position inversely differed from those produced by the left-slanted prism position, in agreement with the simulated results shown in Figure 1. Hence, compared with other general lithographic approaches for fabricating anisotropic nanostructures, this method is simple and promising for tuning the isotropy of geometric features and generating large-area sample homogeneity.

Anisotropic Optical Properties of Anisotropic Metallic Nanoarrays. The novel optical properties of the four types of metallic nanostructures obtained as described above were characterized by calculating the electric field intensity distributions ($|\mathbf{E}|^2$) generated by continuous excitation with a linearly polarized plane wave (λ = 785 nm), which corresponds to the wavelength of the experimental SERS measurement (see Figure S2 in the Supporting Information), using FDTD methods. Here, the intensity enhancement factors ($\eta_I = |\mathbf{E}|^2/|\mathbf{E}_0|^2$) could be obtained by normalizing $|\mathbf{E}|^2$ using the incident wave intensity ($|\mathbf{E}_0|^2$), as shown in Figure 4. The effects of the anisotropic geometries on the LSPR properties were studied using incident excitation with two different orthogonal polarization modes: longitudinal (first row) and transverse (second row) polarizations.[3−5,26−28] Here, the longitudinal and transverse polarizations were perpendicular (⊥) and parallel (=) to the sharp tip axis containing a nanogap. The polarization directions are indicated by the arrows on the simulated results.

A configuration in which the intensities of the three side beams were the same produced a symmetric circular nanohole array with maximum η_I values along the longitudinal (Figure 4a) and transverse (Figure 4e) polarizations that were nearly identical, $10^{0.54}$ and $10^{0.55}$, respectively, near the nanohole rim. The ellipsoidal metallic nanohole arrays yielded different maximum values than the spherical nanoholes: $10^{0.48}$ (Figure 4b) and $10^{0.64}$ (Figure 4f), respectively, due to the anisotropic geometry.[3−5,26−28] The difference was much higher for arrays in which the bridge did not form. Excitation with light polarized

dx.doi.org/10.1021/am402886a | ACS Appl. Mater. Interfaces 2013, 5, 9791−9797

along either of the orthogonal directions yielded maximum η_I values of $10^{1.14}$ (Figure 4c) and $10^{2.91}$ (Figure 4g), respectively. These intense values arose from the combined effects of the presence of sharp corners and nanogaps, both of which yield a strong SERS responses.[5,26−28,30−32] The enhanced EM fields produced by the zigzag-shaped anisotropic nanostructures are, therefore, potentially useful in highly sensitive SERS-based chemical or biomolecule sensing applications (see Figure S2 in the Supporting Information). The maximum η_I values decreased as the prism was further shifted to the left, although the distinction between the longitudinal ($10^{0.21}$, Figure 4d) and transverse ($10^{1.02}$, Figure 4h) polarization modes remained. The decrease in the maximum η_I values mainly resulted from the decrease in the edge sharpness and the increase in the nanogap distance between adjacent nanostructures[27,28,32] rather than the anisotropy. We therefore confirmed that the optical properties of the nanoarrays could be anisotropically tuned by controlling the isotropy of the metallic nanostructure arrays by translating the prism on a sample stage. The tunability of the anisotropic optical properties is expected to be advantageous in electronics, energy, plasmonics, and sensor applications.[1−17]

Anisotropic Polymer Nanowall Arrays and Their Anisotropic Wetting Properties. A two-layer FCC structure etching template could be prepared by the judicious choice of PR thickness.[30−32] The fabrication of isotropic nanotip arrays was previously reported by our research group.[32] HL-derived porous structures having lattice units with a range of polymer bridge thickness values could be fabricated simply using the prism HL method with a left-slanted prism position on the sample stage. The SF_6 RIE process was applied to achieve anisotropic polymer nanowall arrays in which the thin partial polymer bridges were disconnected to form nanogaps. During the etching step, the thin polymer bridges were preferentially disconnected in regions of low cross-linking density (see Figure S5 in the Supporting Information).[32] The nanowall arrays with directional geometric features were thus achieved by the partial removal of thin polymer bridges. Figures 5a and 5b show 30° tilted SEM images of, respectively, isotropic polymer nanotip arrays prepared using a centered prism position and anisotropic polymer nanowall arrays prepared using a left-slanted prism position. The magnified SEM image in the (111) plane (inset of Figure 5b) shows that the anisotropic geometry of the polymer nanowall arrays appears to slant to the left. We designated the direction orthogonal to the nanowall as the *x*-direction and the direction parallel to the nanowall as the *y*-direction.

The wetting properties of the two polymer nanostructure arrays were examined by measuring the contact profiles of water droplets on the nanopatterned surfaces. Figure 5c shows that similar contact angles (CAs) were measured from the polymer nanotip arrays along the orthogonal *x*- and *y*-directions, with values of 116° (θ_x) and 115° (θ_y), respectively. This isotropic wetting property resulted from the symmetric hexagonal order of the nanotips, which displayed directional isotropy. The hydrophobic behavior was attributed to the presence of sharp edges of the surface morphology and the chemical composition of the SF_6 plasma-treated SU-8 surface, which displayed chemically inert fluorinated groups.[29,35] Two-direction anisotropic wetting by the polymer nanowall arrays was demonstrated, as shown in Figure 5d. The water contact profiles displayed distinct CAs for θ_x (116°) and θ_y (98°), unlike the results shown in Figure 5c. Taken together, the two sets of CA measurements were used to define the wetting anisotropy as $\Delta\theta = \theta_x - \theta_y = 18°$. The wetting properties of the nanowall arrays were attributed to the directional anisotropy of the geometrical features, which induced preferential spreading along the nanowalls due to pinning of the water droplet at the nanostructure edges.[6,7,25,29] The anisotropic wetting properties were stable over 5 min, as shown in Figure S6 in the Supporting Information. Although the CA values decreased (θ_x = 75° and θ_y = 58°) due to evaporation and spreading of the water droplets, the $\Delta\theta$ value for the anisotropic nanowall arrays remained high (17°). These results clearly indicated that the polymer nanowall arrays were anisotropic, unlike the symmetric nanotip arrays ($\Delta\theta$ = 2°).

CONCLUSIONS

In summary, we demonstrated a simple and effective approach to fabricate novel anisotropic polymeric/metallic nanoarrays with tunable isotropy. The polymer template was prepared using prism HL in which the prism position was adjusted on a sample stage. The isotropy of the polymer nanohole arrays with hexagonal ordering could be tuned by shifting the prism position to the left or right, relative to the center of the laser beam during HL. As the prism position was shifted further off-center, thin polymer bridges formed from low-intensity regions of the holographic interference patterns, finally disconnected from the structures, as predicted in the simulated results. The anisotropic polymer nanostructures were used as milling masks to easily obtain the corresponding metallic nanostructure arrays. Large-area zigzag-shaped metallic nanoarrays, in which adjacent sharp edges were separated by nanogaps, could be fabricated without defects. The nanogap distance could be controlled by adjusting the degree to which the prism position had been shifted off-center. The resultant metallic nanoarrays displayed anisotropic LSPR properties that depended on the direction of polarization of an incident beam due to the anisotropy of the geometric features. Excitation with a transverse polarized beam (parallel to the sharp tip axis) yielded a maximal η_I value of $10^{2.91}$. Furthermore, bidirectional anisotropic wetting was observed on the anisotropic polymer nanowall array surfaces fabricated by a combination of prism-controlled HL and etching processes. The anisotropic nanoarrays displayed a high degree of anisotropy ($\Delta\theta$ = 18°) with a homeostatic duration of 5 min, in contrast with the isotropically ordered nanotip arrays. Tunable polymeric/metallic nanoarchitectures with anisotropic structures and properties may potentially find utility in a broad array of applications, including electronics, energy, plasmonics, bioengineering, and especially LSPR- or SERS-based sensing devices.

EXPERIMENTAL SECTION

Fabrication of Anisotropic Polymer Nanostructure Arrays. An SU-8 PR formed from a 2:8 solution of resin (EPON SU-8, Miller−Stephenson Chemical) to solvent (γ-butyrolactone (GBL), Sigma−Aldrich) and containing 1 wt % photoinitiator (triarylsulfonium hexafluorophosphate salts, Aldrich) was spin-coated onto a substrate at 2000 rpm over 30 s. The coated substrate was soft-baked on a hot plate at 95°C for 15 min. An expanded laser beam (He−Cd laser, CW, 325 nm, 50 mW, Kimmon, 1 cm beam diameter) was directed through a position-controlled single top-cut prism on a sample stage and directed onto the substrate with a 0.5 s exposure time. The optical setup and specially designed prism is described in detail elsewhere.[30−34] Post-exposure baking was achieved at 55°C for 20 min. Unexposed regions were removed using propylene glycol methyl ether acetate (PGMEA, Aldrich), and the substrate was rinsed with 2-propanol.

Fabrication of the Anisotropic Metallic Nanostructure Arrays. A substrate was prepared by introducing a 30 nm Au coating on the surface. The fabrication steps used to generate the anisotropic polymer nanostructure arrays were then applied as described above. The "messy" SU-8 polymer structures were etched using a 13.56 MHz RF RIE apparatus (Vacuum Science).[30] SF_6 gas was introduced into the chamber at a flow rate of 100 sccm, and etching was performed at a radio frequency (RF) power of 100 W for 1 min. Ar ion milling (10 sccm, ~2 min) with 400 W DC bias was then performed to selectively remove the deposited Au thin film from the vacant spaces on the substrate. The anisotropic Au nanoarrays remained beneath the polymer mask. Finally, O_2 RIE for 5 min under a 100 sccm flow rate and 100 W RF was applied to the prepared samples to remove the polymer masks. The resulting anisotropic metallic nanoarrays exhibited different optical properties, depending on the direction along which the excitation beam was polarized: longitudinal or transverse.

Fabrication of Anisotropic Polymer Nanowall Arrays. Bilayer FCC structures were fabricated using an SU-8 PR with a resin/solvent ratio of 4:6.[30−32] The PR was spin-coated (at 3000 rpm) and soft-baked, a 0.21 s laser exposure was applied through the laterally translated prism. Post-exposure baking and a development process were then applied. Finally, an SF_6 RIE process was applied for 2 min under the experimental conditions described above to disconnect the thin polymer bridges. The resultant anisotropic polymer nanowall arrays showed bidirectional anisotropic wetting properties.

Measurements and Characterization. The morphologies of the sample surfaces were investigated using a field-emission scanning electron microscopy (FESEM) system (Hitachi S-4800). An image analysis program (Image-Pro Plus) was used to automatically determine the thickness of the thin bridges and the nanogaps distance. The water contact angle profiles on the sample surfaces were measured using a contact angle goniometer (KRUSS, DSA 10-Mk2) with 1 μL droplets.

■ ASSOCIATED CONTENT

Ⓢ Supporting Information

Additional simulation, SEM and water profile images, and SERS spectra as described in the text. This information is available free of charge via the Internet at http://pubs.acs.org.

■ AUTHOR INFORMATION

Corresponding Author

*E-mail: smyang@kaist.ac.kr.

Notes

The authors declare no competing financial interest.

■ ACKNOWLEDGMENTS

This work was supported by a grant from the Creative Research Initiative Program of the Ministry of Education, Science and Technology for "Complementary Hybridization of Optical and Fluidic Devices for Integrated Optofluidic Systems".

■ REFERENCES

(1) Tawfick, S.; De Volder, M.; Copic, D.; Park, S. J.; Oliver, C. R.; Polsen, E. S.; Roberts, M. J.; Hart, A. J. *Adv. Mater.* **2012**, *24*, 1628−1674.
(2) Tang, Z.; Wei, A. *ACS Nano* **2012**, *6*, 998−1003.
(3) Cataldo, S.; Zhao, J.; Neubrech, F.; Frank, B.; Zhang, C. J.; Braun, P. V.; Giessen, H. *ACS Nano* **2012**, *6*, 979−985.
(4) Lyvers, D. P.; Moon, J. M.; Kildishev, A. V.; Shalaev, V. M.; Wei, A. *ACS Nano* **2008**, *2*, 2569−2576.
(5) Clark, A. W.; Glidle, A.; Cumming, D. R. S.; Cooper, J. M. *J. Am. Chem. Soc.* **2009**, *131*, 17615−17619.
(6) Xia, D. Y.; Brueck, S. R. J. *Nano Lett.* **2008**, *8*, 2819−2824.
(7) Xia, D. Y.; He, X.; Jiang, Y. B.; Lopez, G. P.; Brueck, S. R. J. *Langmuir* **2010**, *26*, 2700−2706.
(8) Chu, K. H.; Xiao, R.; Wang, E. N. *Nat. Mater.* **2010**, *9*, 413−417.
(9) Marconnett, A. M.; Yamamoto, N.; Panzer, M. A.; Wardle, B. L.; Goodson, K. E. *ACS Nano* **2011**, *5*, 4818−4825.
(10) Liu, S.; Liu, Y.; Cebeci, H.; de Villoria, R. G.; Lin, J. H.; Wardle, B. L.; Zhang, Q. M. *Adv. Funct. Mater.* **2010**, *20*, 3266−3271.
(11) Ok, J. G.; Tawfick, S. H.; Juggernauth, K. A.; Sun, K.; Zhang, Y. Y.; Hart, A. J. *Adv. Funct. Mater.* **2010**, *20*, 2470−2480.
(12) Johansson, F.; Carlberg, P.; Danielsen, N.; Montelius, L.; Kanje, M. *Biomaterials* **2006**, *27*, 1251−1258.
(13) Hurtado, A.; Cregg, J. M.; Wang, H. B.; Wendell, D. F.; Oudega, M.; Gilbert, R. J.; McDonald, J. W. *Biomaterials* **2011**, *32*, 6068−6079.
(14) Zhang, G.; Wang, D. Y.; Mohwald, H. *Nano Lett.* **2007**, *7*, 3410−3413.
(15) Yang, J. K. W.; Jung, Y. S.; Chang, J. B.; Mickiewicz, R. A.; Alexander-Katz, A.; Ross, C. A.; Berggren, K. K. *Nat. Nanotechnol.* **2010**, *5*, 256−260.
(16) Lee, S.; Shin, J.; Lee, Y. H.; Fan, S.; Park, J. K. *Nano Lett.* **2010**, *10*, 296−304.
(17) Lee, S.; Kang, H. S.; Park, J. K. *Adv. Funct. Mater.* **2011**, *21*, 1770−1778.
(18) Campbell, M.; Sharp, D. N.; Harrison, M. T.; Denning, R. G.; Turberfield, A. J. *Nature* **2000**, *404*, 53−56.
(19) Cai, L. Z.; Yang, X. L.; Wang, Y. R. *Opt. Lett.* **2002**, *27*, 900−902.
(20) Su, H. M.; Zhong, Y. C.; Wang, X.; Zheng, X. G.; Xu, J. F.; Wang, H. Z. *Phys. Rev. E* **2003**, *67*, 056619.
(21) Pang, Y. K.; Lee, J. C. W.; Lee, H. F.; Tam, W. Y.; Chan, C. T.; Sheng, P. *Opt. Express* **2005**, *13*, 7615−7620.
(22) Moon, J. H.; Yang, S. M.; Pine, D. J.; Chang, W. S. *Appl. Phys. Lett.* **2004**, *85*, 4184−4186.
(23) Lu, C.; Hu, X. K.; Dimov, S. S.; Lipson, R. H. *Appl. Optics* **2007**, *46*, 7202−7206.
(24) Danh, B. D.; Ngoc, D. L.; Wu, C. Y.; Lin, J. H.; Hsu, C. C. *Appl. Optics* **2011**, *50*, 579−585.
(25) Wu, S. Z.; Wu, D.; Yao, J.; Chen, Q. D.; Wang, J. N.; Niu, L. G.; Fang, H. H.; Sun, H. B. *Langmuir* **2010**, *26*, 12012−12016.
(26) Bochenkov, V. E.; Sutherland, D. S. *Nano Lett.* **2013**, *13*, 1216−1220.
(27) Hatab, N. A.; Hsueh, C. H.; Gaddis, A. L.; Retterer, S. T.; Li, J. H.; Eres, G.; Zhang, Z. Y.; Gu, B. H. *Nano Lett.* **2010**, *10*, 4952−4955.
(28) Dodson, S.; Haggui, M.; Bachelot, R.; Plain, J.; Li, S.; Xiong, Q. *J. Phys. Chem. Lett.* **2013**, *4*, 496−501.
(29) Park, S. G.; Moon, J. H.; Jeon, H. C.; Yang, S. M. *Soft Matter* **2012**, *8*, 4567−4570.
(30) Jeon, H. C.; Heo, C. J.; Lee, S. Y.; Yang, S. M. *Adv. Funct. Mater.* **2012**, *22*, 4268−4274.
(31) Jeon, H. C.; Heo, C. J.; Lee, S. Y.; Park, S. G.; Yang, S. M. *J. Mater. Chem.* **2012**, *22*, 4603−4606.
(32) Jeon, H. C.; Park, S. G.; Cho, S.; Yang, S. M. *J. Mater. Chem.* **2012**, *22*, 23650−23654.
(33) Lee, S. K.; Park, S. G.; Moon, J. H.; Yang, S. M. *Lab Chip* **2008**, *8*, 388−391.
(34) Kang, J. H.; Moon, J. H.; Lee, S. K.; Park, S. G.; Jang, S. G.; Yang, S.; Yang, S. M. *Adv. Mater.* **2008**, *20*, 3061−3065.
(35) Park, S. G.; Lee, S. Y.; Jang, S. G.; Yang, S. M. *Langmuir* **2010**, *26*, 5295−5299.